1-1-2010

Ni doping of semiconducting boron carbide

Nina Hong
University of Nebraska - Lincoln

Marjorie Langell
University of Nebraska - Lincoln, mlangell1@unl.edu

Jing Liu
University of Nebraska - Lincoln

Orhan Kizilkaya
Louisiana State University, 6980 Jefferson Highway, Baton Rouge, Louisiana

S. Adenwalla
University of Nebraska - Lincoln, sadenwalla1@unl.edu

Ni doping of semiconducting boron carbide

Nina Hong (이니나),[1] M. A. Langell,[2] Jing Liu,[1] Orhan Kizilkaya,[3] and S. Adenwalla[1,a)]
[1]*Department of Physics and Astronomy, University of Nebraska-Lincoln, Lincoln, Nebraska 68588-0511, USA*
[2]*Department of Chemistry, University of Nebraska-Lincoln, Lincoln, Nebraska 68588-0304, USA*
[3]*Center for Advanced Microstructures and Devices, Louisiana State University, 6980 Jefferson Highway, Baton Rouge, Louisiana 70806, USA*

(Received 21 August 2009; accepted 7 December 2009; published online 27 January 2010)

The wide band gap, temperature stability, high resistivity, and robustness of semiconducting boron carbide make it an attractive material for device applications. Undoped boron carbide is p type; Ni acts as a n-type dopant. Here we present the results of controlled doping of boron carbide with Ni on thin film samples grown using plasma enhanced chemical vapor deposition. The change in the dopant concentration within the thin film as a function of the dopant flow rate in the precursor gas mixture was confirmed by x-ray photoelectron spectroscopy measurements; with increasing dopant concentration, current-voltage (I-V) curves clearly establish the trend from p-type to n-type boron carbide. © *2010 American Institute of Physics*. [doi:10.1063/1.3284205]

I. INTRODUCTION

In the development of a semiconductor, the ability to control both n- and p-type doping is of paramount importance for device applications.[1] The development of a semiconducting form of boron carbide has resulted in heterojunction diodes, a junction gate field-effect-transistor (JFET),[2] Esaki-type tunnel diodes,[3] homojunction diodes, heterojunction neutron detectors,[4,5] and a high temperature heterojunction diode with SiC.[6] Semiconducting boron carbide devices have been found to be valuable in a variety of unique device applications. Chief among them are solid state neutron detectors due to the high cross section of ^{10}B for thermal neutrons[7] and the ability to both capture neutrons and sweep out charge in the same material. In addition, the high resistivity and dielectric constant of boron carbide ($\sim$8) make it eminently suitable as a tunneling barrier for magnetic tunnel junctions. Photoemission studies of boron carbide/Co interfaces show no quenching of the Co magnetic moment at the interface, an important consideration for spintronic applications.[8] Controlled doping of the boron carbide barrier layer will allow for precise positioning of the Fermi level, hence changing the tunneling characteristics.

In the absence of intentional doping, boron carbide is a p-type semiconductor with a resistivity of $\sim 10^{10}$ Ω cm at room temperature. Ni has been found to be an excellent n-type dopant,[9,3] and boron carbide homojunction diodes have been made using Ni doped n-type and undoped p-type boron carbide. In this letter, we report on the controlled doping of semiconducting boron carbide. The correlation between increasing Ni concentration and n-type semiconducting characteristics is confirmed by x-ray photoelectron spectroscopy (XPS) and I-V measurement. Ni doping results in a significant upward shift of the Fermi level and does not lead to significant changes in the surface quality; however, x-ray diffraction (XRD) results indicate a change in the crystallinity.

II. EXPERIMENTAL DETAILS

The plasma enhanced chemical vapor deposition (PECVD) growth of semiconducting boron carbide films has been well documented.[6] PECVD lends itself quite easily to good control of the dopant density if a suitable precursor molecule can be found. $C_2B_{10}H_{12}$ (orthocarborane) is used as the precursor molecule for boron carbide deposition, and $Ni(C_5H_5)_2$ (nickelocene)[10] as the source molecule for introduction of the Ni dopant. A vial of nickelocene in parallel with the orthocarborane vial (at a temperature of 90 °C) is inserted into the gas handling system and maintained at a temperature of 27 °C. The argon gas flow through the two vials is varied, as shown in Table I. The ratio of the two precursors in the mix will depend on the respective vapor pressures and inlet and outlet tube geometries and must be a monotonic function of the relative gas flows since all other variables remain unchanged. The vapor pressures of nickelocene and orthocarborane as a function of temperature are well known,[11,12] giving a ratio of 0.001 135 atoms of Ni per molecule of orthocarborane ($\sim$0.11%) for a dilution ratio of 1. For all other dilution ratios, the proportion of Ni in the gas mix will rise in proportion to the argon gas flow. Hence for the 9:1 dilution ratio, the incoming gas will contain 1% of Ni. Two series of samples were made, one on n-type Si with a measured resistivity of 100 Ω cm corresponding to a dopant density of 4.5×10^{13} cm^{-3} and one on p-type Si with a resistivity of 16 Ω cm corresponding to a dopant density of 1×10^{15} cm^{-3}. At each dilution ratio, the samples on the n-type and p-type Si were grown simultaneously in the same chamber; hence we expect the film compositions on the two different substrates to be identical. X-ray reflectivity data, which are not shown, indicated the same growth rate ($\sim$10 nm/min) for each sample when the Ar flow rate through the orthocarborane vial is fixed. Substrates were

a)Author to whom correspondence should be addressed. Electronic mail: sadenwalla1@unl.edu.

TABLE I. Ar gas flow through the orthocarborane and nickelocene vials for all samples. The dilution ratio is defined as the ratio of Ar gas flow through the nickelocene vial to Ar gas flow through the orthocarborane vial. The Ni concentration in the gas phase increases with increasing dilution ratio.

Sample name	BC	Ni(1)-BC	Ni(3)-BC	Ni(5)-BC	Ni(7)-BC	Ni(9)-BC
Orthocarborane	1 SCCM	1 SCCM	1 SCCM	1 SCCM	1 SCCM	1 SCCM
Nickelocene	0 SCCM	1 SCCM	3 SCCM	5 SCCM	7 SCCM	9 SCCM
Dilution ratio	0	1	3	5	7	9

cleaned using acetone, methanol, de-ionized water, and 5% HF before insertion into the PECVD reactor. Inside the reactor, a 30 min Ar ion etch was performed prior to deposition. All samples were deposited at a substrate temperature of 330 °C for 1 h, leading to films that are 600 nm thick.

The structural properties of undoped and doped boron carbide were compared by atomic force microscope (AFM) and θ-2θ XRD scans using Cu Kα radiation ($\lambda = 1.54$ Å) at room temperature. The relative Ni concentrations as a function of the Ni source molecule's flow rate were investigated by XPS measurements using a Physical Electronics 04-548 dual x-ray anode with unmonochromatized Mg Kα radiation. The photoemission was energy analyzed with an Omnicron EA 125 concentric hemispherical analyzer operating at a constant pass energy of 15 eV for carbon, boron, and oxygen, and 50 eV for nickel. The spectra were taken in 0.1 eV increments and were averaged for 25–50 scans. Binding energies were calibrated to adventitious carbon, with C1s taken to be 284.6 eV. *In situ* surface treatment could be performed with inert ion bombardment with a Physical Electronics 04-303 differentially pumped ion source. Ion sputtered substrates were treated using 3 kV Ar^+ in normal incidence mode for 40 min, leading to the removal of ~20 nm of surface material. The x-ray absorption near edge structure (XANES) spectra were undertaken at the double crystal monochromator (DCM) beamline at the Center for Microstructures and Devices (CAMD). Monochromatic light was obtained by using a DCM of Lemonnier type,[13] equipped with Ge(220) crystal pair with an overall resolution of ~2 eV. The fluorescence yield mode utilizing a Canberra 13-element high purity germanium diode array detector was used to collect the XANES data. The monochromator was calibrated at the Ni K edge at 8333 eV using a Ni foil.

The variations in semiconducting properties were established from the I-V curves of each heterojunction diode. Circular Ohmic Cr/Au contacts with diameters ranging from 1 to 5 mm were sputter deposited on both sides of the boron carbide/Si heterojunction.

III. RESULTS AND DISCUSSION

The structure of the interface is an important parameter in the development of tunnel junctions and homojunction diodes. The AFM images of undoped (left) and highly doped (right) boron carbide films on Si substrates in Fig. 1 indicate rms roughnesses of 2.1 and 2.5 nm, respectively. High dopant concentrations have no discernible effect on the surface roughness, leading us to conclude that PECVD is a viable method for the growth of homojunction diodes and highly doped tunnel junctions.

XRD scans are shown in Fig. 2 for a subset of the samples. The undoped and lightly doped films show x-ray peaks at $2\vartheta \sim 23.5°$ and 43° and typical crystallite sizes of ~10 nm, substantially less than the film thickness of 600 nm.[6] Two key differences between these two films are observed: in the undoped film, the peak at 43° consists of two

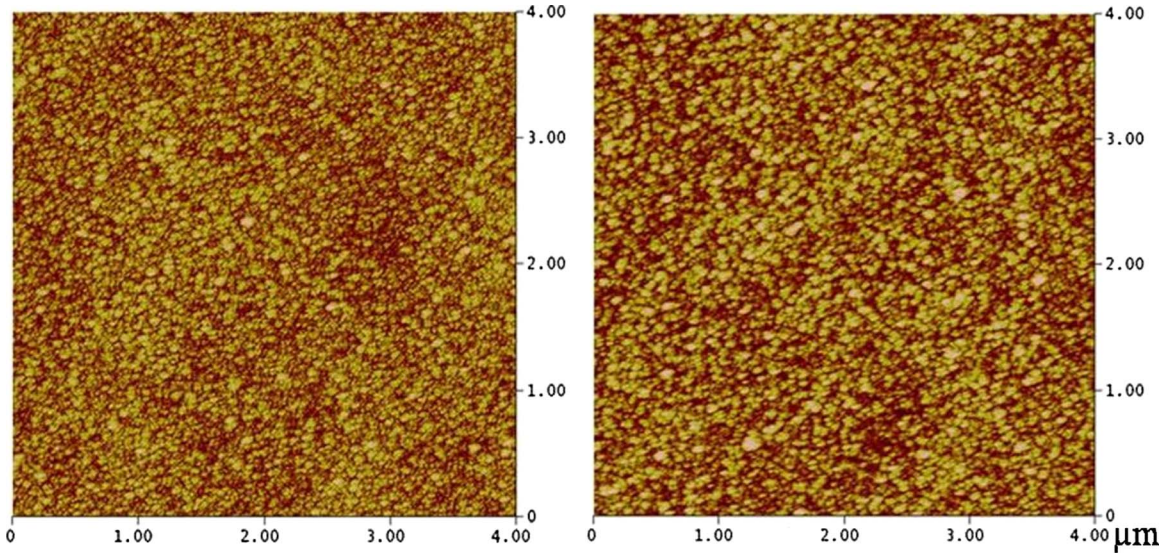

FIG. 1. (Color online) AFM images for BC (left) and Ni(9)-BC (right) on Si substrates, showing no significant change in the surface quality. rms roughness values are 2.1 nm for BC and 2.5 nm for Ni(9)-BC. The z range is 15 nm.

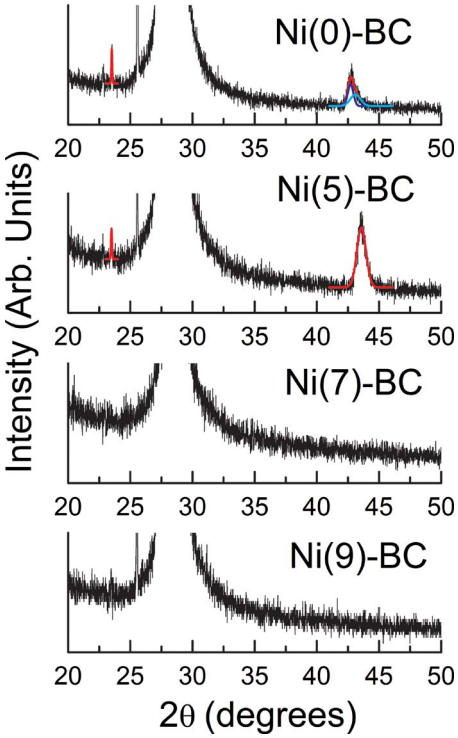

FIG. 2. (Color online) XRD data for Ni(0, 5, 7, and 9)-BC films on Si substrates over a selected region (20°–50°) chosen to optimally display the BC peaks. The Si (111) and SiO_2 peaks are at 28.5° and 25.5°, respectively. Undoped BC and Ni(5)-BC show diffraction peaks at 23.5° and 43°. The peak at 43° in the undoped sample consists of two peaks at 42.7° and 43.0° with almost equal intensities. In the Ni(5)-BC sample, a single peak at 43.59° is seen. The relative intensities of the x-ray peaks are obtained from Gaussian fits shown. No peaks are seen for Ni(7)-BC and Ni(9)-BC.

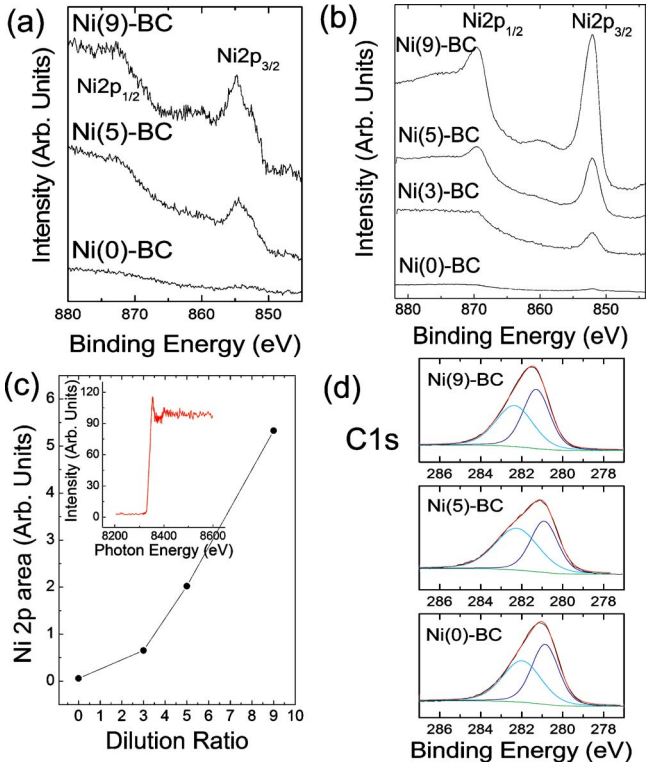

FIG. 3. (Color online) Ni2p XPS spectrum (a) before and (b) after sputtering to remove surface contaminants. Measurements of the surface before sputtering indicate the presence of NiO. After sputtering, the peak shape is similar to that of metallic Ni. (c) Plot of the Ni2p peak area as a function of dilution ratio. The Ni peak intensity is normalized to the area under the corresponding B1s peak. Increasing the ratio of Ni in the gas phase leads to a corresponding increase in Ni concentration in the thin films. The inset shows the XANES data of a Ni(7)-BC thin film, showing the Ni edge close to the expected energy of 8333 eV. (d) C1s XPS spectrum after sputtering, showing the absence of graphitic carbon in both undoped and Ni doped boron carbide.

barely resolved peaks at 42.7° and 43°, whereas in the lightly doped sample, only a single peak at 43.59° is seen. The ratio of the intensities of the two peaks (at 43° and 23°) changes from ~7.5 for the undoped sample to 17 for the lightly doped sample. The more highly doped BC films show no XRD peaks, implying that the addition of Ni leads to yet further disruption of the crystalline structure. Similar effects have been seen in sputtered semiconducting thin films and have been attributed to decreasing crystallite size with increasing dopant concentration.[14] Identification of the crystal structures of boron carbide based on x-ray data is fraught with difficulty, owing to the plethora of similar crystal structures that may differ only in the placement of C atoms and/or small differences in the size of the unit cell (and hence the position of the diffraction peak). All are based on the structure of icosahedral B, with the icosahedra at the corners and/or faces of rhombohedral and tetrahedral unit cells. Restricting ourselves to a single polytype, the positions of the split peak at 43° for the undoped sample and the peak at 23° indicate a structure similar to the crystal structure for orthorhombic B_8C.[15] Differences in the relative intensities as compared to the powder pattern may be attributed either to a preferential growth direction or to the presence of two C atoms in the icosahedra from the precursor molecule. At low levels of Ni doping, the crystallite sizes are not reduced, but the change in the relative intensities may imply a change in the preferred orientation. n-type doping of rhombohedral boron with transition metal elements[16] in powder samples indicates that the transition metal elements enter interstitial sites, while maintaining the overall crystal structure, at concentrations far higher than in the present samples. Extended x-ray-absorption fine structure and XANES measurements of Co doped boron carbide at concentrations of ~1% (Ref. 17) are consistent with Co atoms replacing one of the icosahedral atoms. As we shall show below, the Ni atom concentrations in the present samples are well below this range, and hence structural information on the position of the Ni atoms is hard to obtain.

To investigate the presence of Ni atoms in the semiconducting thin film, both XPS and XANES measurements are shown in Fig. 3. The Ni2p region shown in Fig. 3(b) was obtained after Ar ion sputtering, showing peaks that are characteristic of metallic Ni with low satellite structure and binding energies of $2p_{3/2}=852.1$ eV and $2p_{1/2}=869.5$ eV comparable to literature spectra for the metal,[18] consistent with the interstitial sites shown previously for transition metal dopants.[16,19] Similar measurements taken before surface sputtering [Fig. 3(a)] showed the existence of NiO with $2p_{3/2}=854.5$ eV and $2p_{1/2}=872.2$ eV and strong, characteristic satellite structure, indicating the presence of surface oxides. To calculate relative surface concentrations, the $Ni2p_{3/2}$

peak in the sputtered samples is normalized by the total area of the B1s peak intensity obtained on the same sample and this normalized peak intensity is shown in Fig. 3(c) as a function of the nickelocene flow rate. Since a fixed Ar flow rate through the orthocarborane vial was used (resulting in the same growth rate for each sample), we assume a constant quantity of boron within the film. The undoped sample shows Ni peak intensities barely above the noise level. As the nicklocene ratio increases, so too does the relative Ni concentration, leading us to conclude that the atomic ratios in the thin film are essentially proportional to the gas phase ratios. XANES measurements of the characteristic absorption edge of nickel at a value close to the expected 8333 eV of the Ni K edge are shown in the inset of Fig. 3(c) on the 7:1 sample, providing additional confirmation of the presence of Ni within the film. The shape of the signal is distinct from that of pure Ni, indicating hybridization of the Ni atoms. Exact details of the hybridization will require samples with much higher doping levels. The detection limit for this XANES setup is 10 ppm, and an order of magnitude estimate of the amount of Ni in the sample indicates a level of ~0.1%, significantly reduced from the proportion of Ni atoms in the precursor gas mix, which is calculated at close to 0.8%. These minute quantities of dopant atoms have a significant effect on the electronic properties, a characteristic of doping, quite distinct from the Co and Fe doped BC films,[19] with far higher impurity concentrations of ~1% within the film.

Concerns regarding the C content of the nickelocene precursor molecule and its effects on the BC structure were probed by XPS measurements of the C1s peak as a function of Ni doping. We looked for both an increase in graphitic carbon and changes in the icosahedral cage. Figure 3(d) shows C1s peaks for the Ni(0, 5, 9)-BC samples after Ar^+ ion sputtering. Each peak was fitted (using a 25% Lorentzian–Gaussian function) to two separate peaks. The first peak at 281.0 eV corresponds to the C–B–C chain and the second peak at 282.2 eV corresponds to the $B_{11}C$ icosahedral cage.[20,21] There is no substantial change in the ratio or position of the two peaks on increasing the Ni concentration from 0 to the highest doped 9:1 sample. Moreover, unlike sputter deposited BC films,[20,21] these PECVD grown boron carbide films do not show the presence of the characteristic graphite peak at ~284.4 ± 0.2 eV, either with or without the addition of Ni. This is consistent with the much higher resistivity of the PECVD (Ref. 22) grown samples as compared to hot-pressed[23] and sputter deposited[20,21] BC samples.

With increased concentrations of dopant atoms, distinct changes in the electronic properties are apparent in the room temperature I-V curves of the complete series of heterojunction diodes, as shown in Fig. 4. Positive voltage is applied to the p-type layer, i.e., boron carbide layer (p-type Si layer) in the left (right) panel. The figure dramatically illustrates the effect of increased doping. Undoped boron carbide on n-type Si forms excellent diodes. Looking from top to bottom in the left panel for n-type Si substrates, the diode quality worsens with increased Ni doping, until at a dilution ratio of 1:9, the I-V curve reverses. In contrast, in the right panel for p-type Si substrates, the diode properties *improve* with increased Ni doping. Clearly, increasing the concentration of Ni results in a substantial increase in n-type character.

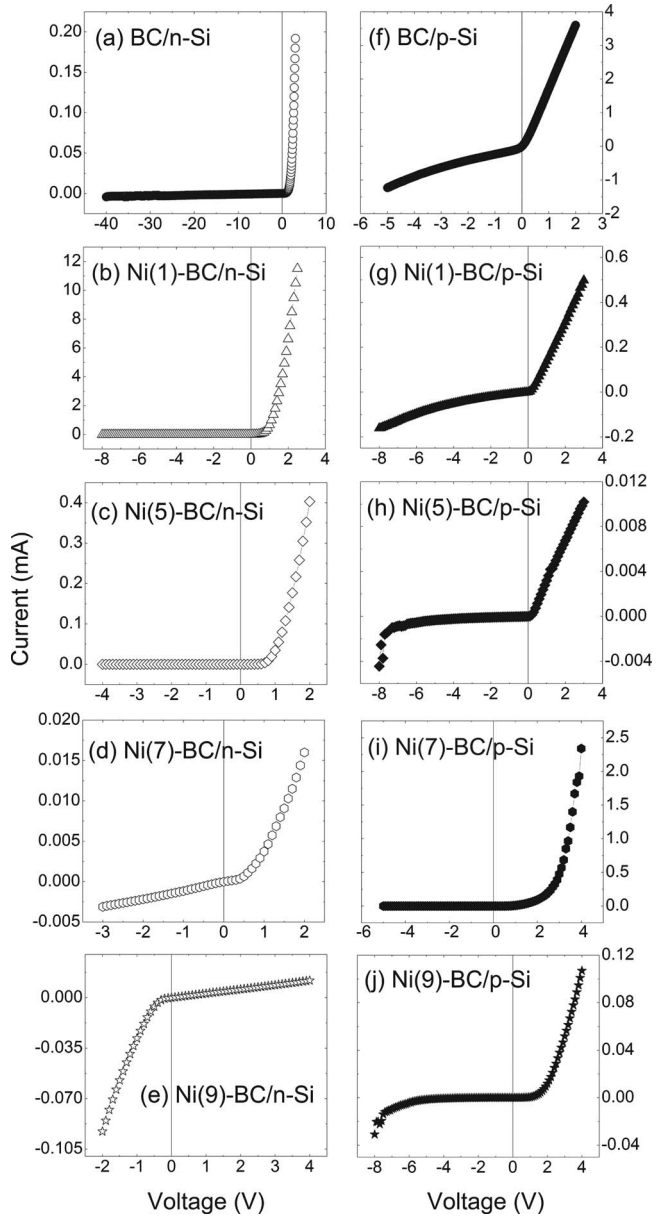

FIG. 4. Current-voltage (I-V) curves of Ni(X)-BC (X=0, 5, 7, and 9) on n-type Si [(a)–(e) left hand column] and on p-type Si [(f)–(j) right hand column] at room temperature, showing clear evidence for the trend toward n-type behavior at higher doping concentrations.

The forward biased turn on voltage V_{bi} is a measure of the difference in Fermi levels between two isolated semiconductors; in our case, Si and BC changes in V_{bi} reflect a change in the Fermi level, a signature of doping. The net increase in V_{bi} in going from the undoped, p-type BC to the highest Ni doping concentration is 0.8 V, raising the Fermi level by 0.8 eV, a significant fraction of the optically measured band gap of 2.2 eV in BC. In terms of energies,

$$qV_{bi} = q\chi^{BC} + (E_c{}^{BC} - E_F{}^{BC}) - [q\chi^{Si} + (E_c{}^{Si} - E_F{}^{Si})], \quad (1)$$

where χ, E_C, and E_F are the electron affinities, the conduction band energies, and the Fermi levels in each semiconductor.

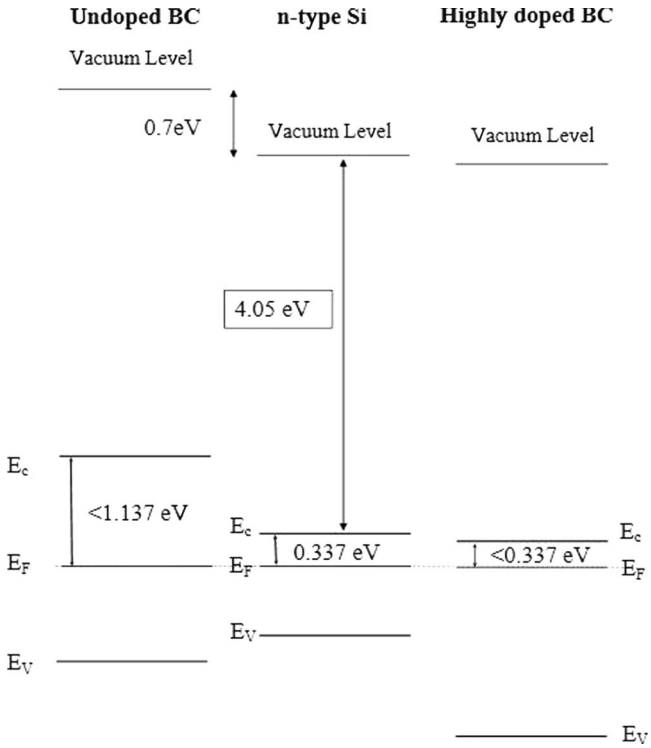

FIG. 5. Energy band diagram of undoped BC, n-type Si, and highly Ni doped BC. The electron affinity for BC is unknown. The constraints on the positions of the Fermi level in the BC arise from the behavior of the I-V curves with increased doping. All quantities for the Si substrate are well known. For details see text.

Although the electron affinity and the position of the Fermi level are not known for the BC film, we can tentatively draft a possible band structure for the Si/BC heterojunction diodes if we assume that the electron affinity and band gap do not change with doping, i.e., that we are in the nondegenerate limit. For the BC on n-type Si—the I-V curves in the left column—the diode curve reverses at the highest doping concentration studied, providing an important quantifiable piece of evidence for placement of the energy bands. The Fermi level for the n-type Si substrate is 0.337 eV below the conduction band. The Fermi level for the BC film is below this level until a doping concentration corresponding to a dilution ratio of >7 is reached. At a dilution ratio of 9, the I-V curve reverses, implying that it is now easier for electrons to diffuse from the BC to the Si. Together with the knowledge of the band gap of BC and the shift in the Fermi level upward by 0.8 eV, the final Fermi levels are tightly constrained and are shown graphically in Fig. 5 for the BC/Si heterojunction. At equilibrium, the Fermi levels are constant across the heterojunction. The I-V curve indicates that E_c^{BC} is higher than E_c^{Si} until a dilution ratio of 9 is reached, at which point the Fermi level in the BC has shifted upward toward the conduction band by 0.8 eV and E_C^{BC} is lower than E_c^{Si}. Algebraically, we can express this as

$$(E_c - E_F)_{\text{for undoped BC}} - 0.8\ \text{eV} < (E_c - E_F)_{\text{for the given n-type Si}}, \tag{2}$$

which implies that for undoped BC the Fermi level can be *at most* 0.037 eV below midgap, very close to intrinsic (note that we have neglected the effects of the interface dipole potential, a correction which amounts to ~0.1 eV for most heterojunctions[24]). A similar structure for the p-type Si substrate, in which the Fermi level is 0.245 eV above the valence band, may also be constructed.

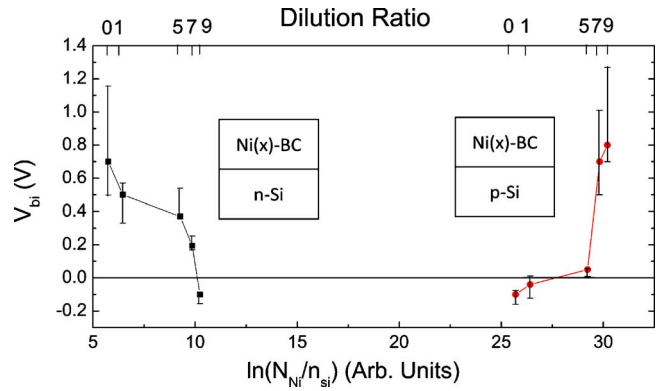

FIG. 6. (Color online) The plots of built-in potential vs natural log of relative Ni concentration normalized by the electron carrier concentration of n- (or p)-type Si. The top scale shows the dilution ratio, increasing to the right. Since n_{Si} for the p-type Si substrate is much smaller than that for the n-type substrate, all data on the p-type Si are shifted to the right. The nonlinearity of these curves indicates that the carrier concentration n in the BC layer is not proportional to the dopant concentration N_D.

For crystalline heterojunction diodes in the nondegenerate limit, the relationship between the energy levels and doping concentrations is straightforward and V_{bi} is given by

$$V_{bi} = \Delta\chi + \frac{kT}{q}\ln\left[\frac{n_n N_{c,p}}{n_p N_{c,n}}\right], \tag{3}$$

where $\Delta\chi$ is the difference in electron affinity values, n_n (n_p) are the electron carrier concentrations, and $N_{c,n}(N_{c,p})$ are the effective density of states at the conduction band edge on the n(p) sides of the junction. A similar expression exists for the hole concentration and the density of states at the valence band. The relative increase in carrier concentration is apparent in Fig. 6, a plot of V_{bi} versus the log of the relative Ni concentration (as obtained from XPS) normalized to the Si carrier density.

For the junctions on n-type Si, we can rewrite Eq. (3) as

$$V_{bi} = -\Delta\chi - \frac{kT}{q}\ln\left[\frac{N_{c,Si}}{N_{c,BC}}\right] - \frac{kT}{q}\ln\left[\frac{n_{BC}}{n_{Si}}\right], \tag{4}$$

and for those on p-type Si

$$V_{bi} = \Delta\chi + \frac{kT}{q}\ln\left[\frac{N_{c,Si}}{N_{c,BC}}\right] + \frac{kT}{q}\ln\left[\frac{n_{BC}}{n_{Si}}\right]. \tag{5}$$

V_{bi} is plotted against the natural log of the relative Ni concentration obtained from XPS, normalized to the electron carrier concentration of n- or p-type Si. Assuming that Ni doping leaves both the electron affinity and the density of states unchanged and that the n-type carrier concentration in BC is a linear function of the Ni concentration, both sets of data should lie on straight lines with a negative slope for the diodes on n-type Si and a positive slope for those on p-type Si. Clearly, this is not the case, leading to the conclusion of a more complex relationship between the Fermi level and doping concentration. Even in the case of purely crystalline

semiconductors, $N_D = n$ is only true when $N_D \gg N_A$. In the case of doped BC, in which the undoped material has p-type characteristics, there must be doping concentrations at which $N_D \approx N_A$, in which case the entire expression for

$$n = \frac{N_D^+ - N_A^-}{2} + \sqrt{\left(\frac{N_D^+ - N_A^-}{2}\right)^2 + n_i^2} \quad (6)$$

is necessary. In the case of amorphous and microcrystalline semiconductors in which there exists a small albeit finite density of states in the gap, the shift in the Fermi level due to doping is dominated by the expression

$$N_D^+ = \int \frac{g(\varepsilon)}{1 + e^{(\varepsilon - \varepsilon_F)}} d\varepsilon, \quad (7)$$

where N_D^+ is the density of fully ionized dopants in the semiconductor[25] and the limits of integration extend from the Fermi level of the undoped semiconductor to the conduction band edge. In these semiconductors, changes in the electronic properties arise from changes in the occupation of states within the gap. Paradoxically, as elucidated by Spear,[25] in order for small concentrations of dopant atoms to produce visible changes in the electronic properties, it is necessary that the density of states in the gap is low. Preliminary photoemission measurements of this entire series of samples indicate minimal tailing and a well-defined gap with a negligible density of states within the gap.

Complex doping mechanisms have been noted in amorphous,[26] microcystalline,[27] and polycrystalline Si (Ref. 28) in which the interaction between dopant atoms, local defects, and hydrogen passivation controls the doping efficiency. Hydrogen plays an important role in passivating defects, thus enabling the structural sensitivity necessary for doping in the amorphous material. In polycrystalline Si, at low dopant atom concentrations, there is no change in carrier concentration; the dopant atoms play the role of defect compensation, and changes in carrier concentrations are noted only at higher dopant atom concentrations. As is the case in Si:H, the CVD growth process for doping boron carbide using hydrogen rich precursor gases (specifically nickelocene) is the potential source for the introduction of hydrogen into the film. We note, however, that in previous experiments using PECVD grown films of BC doped with nickelocene, IR measurements indicate no significant increase in the intensity of the BH or CH bond with doping, implying at best only a small increase in the H concentration.[3] Doping effects are readily apparent at rather low levels of doping, implying that defect compensation plays a minor role. Further measurements of the density of gap states, the electron affinity, and the band structure are necessary to elucidate the doping mechanism.

IV. CONCLUSIONS

We have demonstrated controlled doping of semiconducting boron carbide thin films grown by PECVD using Ni as a n-type dopant. The overall trend from p to n was investigated as a function of dilution ratio which was controlled by the source molecule's flow rate. Doping does not affect the surface roughness but does alter the crystal structure. Incorporation of Ni into the BC film was shown to be relatively inefficient; however, even these small quantities of dopant are shown to notably affect the electronic properties. Over the range of doping investigated, there is a significant change in the position of the Fermi level as measured by the built-in voltage. The controlled doping of semiconducting boron carbide over this large range is extremely promising for future applications in neutron detectors and magnetic tunnel junctions.

ACKNOWLEDGMENTS

This research at UNL was supported by the NASA under Grant Nos. NNG05GM89G and NSF-0725881, the Defense Threat Reduction Agency (Grant No. HDTRA1-09-1-0060), and also the Nebraska Research Initiative. The operation of CAMD is supported by the State of Louisiana. We would like to acknowledge the staff of CAMD for their support in the XANES studies.

[1] G. Braunstein, A. Muraviev, H. Saxena, N. Dhere, V. Richter, and R. Kalish, Appl. Phys. Lett. **87**, 192103 (2005).
[2] D. Byun, B. R. Spady, N. J. Ianno, and P. A. Dowben, Nanostruct. Mater. **5**, 465 (1995).
[3] D. N. McIlroy, S.-D. Hwang, K. Yang, N. Remes, P. A. Dowben, A. A. Ahmad, N. J. Ianno, J. Z. Li, J. Y. Lin, and H. X. Jiang, Appl. Phys. A: Mater. Sci. Process. **67**, 335 (1998).
[4] B. W. Robertson, S. Adenwalla, A. Harken, P. Welsch, J. I. Brand, P. A. Dowben, and J. P. Claassen, Appl. Phys. Lett. **80**, 3644 (2002).
[5] E. Day, J. Diaz, and S. Adenwalla, J. Phys. D: Appl. Phys. **39**, 2920 (2006).
[6] S. Adenwalla, P. Welsch, A. Harken, J. I. Brand, A. Sezer, and B. W. Robertson, Appl. Phys. Lett. **79**, 4357 (2001).
[7] D. S. McGregor, S. M. Vernon, H. K. Gresch, S. M. Markham, S. J. Wojtczuk, and D. K. Wehe, IEEE Trans. Nucl. Sci. **47**, 1364 (2000).
[8] L. Bernard, A. N. Caruso, B. Xu, B. Doudin, and P. A. Dowben, Thin Solid Films **428**, 253 (2003).
[9] S.-D. Hwang, N. B. Remmes, D. N. McIlroy, and P. A. Dowben, J. Vac. Sci. Technol. B **14**, 2957 (1996).
[10] Sigma-Aldrich, http://www.sigmaaldrich.com.
[11] L. A. Torres-Gómez, G. Barreiro-Rodriguez, and F. Mendez-Ruiz, Thermochim. Acta **124**, 179 (1988).
[12] H. A. Pathak, P. M. Raole, C. Jariwala, P. Semwal, and Y. C. Saxena, Fusion Engineering 2005, 21st IEEE/NPS Symposium, 2005 (unpublished), pp. 1–4.
[13] M. Lemonnier, O. Collet, C. Depautex, J. M. Esteva, and D. Raoux, Nucl. Instrum. Methods Phys. Res. A **152**, 109 (1978).
[14] M. Becerril, O. Zelaya-Angel, R. Ramirez-Bon, F. J. Espinoza-Beltran, and J. Gonzalez-Hernandez, Appl. Phys. Lett. **70**, 452 (1997).
[15] K. Ploog and M. Druminski, Krist. Tech. **9**, 25 (1974).
[16] H. Werheit, R. Schmechel, V. Kueffel, and T. Lundstrom, J. Alloys Compd. **262–263**, 372 (1997).
[17] A. Yu. Ignatov, Ya. B. Losovyj, L. Carlson, D. LaGraffe, J. I. Brand, and P. A. Dowben, J. Appl. Phys. **102**, 083520 (2007).
[18] C. D. Wagner, W. M. Rigg, L. E. Davis, J. F. Moulder, and G. E. Mullenberg, *Handbook of X-Ray Photoelectron Spectroscopy* (Physical Electronics, Eden Prairie, MN, 1979).
[19] P. A. Dowben, O. Kizilkaya, J. Liu, B. Montag, K. Nelson, I. Sabirianov, and J. I. Brand, Mater. Lett. **63**, 72 (2009).
[20] I. Jiménez, L. J. Terminello, F. J. Himpsel, M. Grush, and T. A. Callcot, J. Electron Spectrosc. Relat. Phenom. **101–103**, 611 (1999).

[21]I. Jiménez, D. G. J. Sutherland, T. van Buuren, J. A. Carlisle, L. J. Terminello, and F. J. Himpsel, Phys. Rev. B **57**, 13167 (1998).
[22]S. Lee, J. Mazurowski, R. Ramseyer, and P. A. Dowben, J. Appl. Phys. **72**, 4925 (1992).
[23]C. Wood and D. Emin, Phys. Rev. B **29**, 4582 (1984).
[24]W. R. Frensley and H. Kroemer, Phys. Rev. B **16**, 2642 (1977).
[25]W. E. Spear, Adv. Phys. **26**, 811 (1977).
[26]W. B. Jackson, Phys. Rev. B **41**, 12323 (1990).
[27]W. E. Spear, G. Willeke, P. G. LeComber, and A. G. Fitzgerald, J. Phys. (Paris) **42**, C4 (1981).
[28]M. Taniguchi, M. Hirose, Y. Osaka, and S. Hasegawa, Jpn. J. Appl. Phys. **19**, 665 (1980).